On a pore-scale film flow approach to describe moisture transfer in a hygroscopic porous medium

M. Goyeneche [a],[*], D.M. Bruneau [a], D. Lasseux [a], B. Desbat [b],[1], J.P. Nadeau [a]

[a] L.E.P.T.-ENSAM, Esplanade des Arts et Métiers, 33405 Talence Cedex, France
[b] L.P.C.M., 351 Cours de la Libération, 33405 Talence Cedex, France

Abstract

In this work, a film flow model is developed to describe free water transport in a network of parallel capillaries. This model is inserted in a numerical drying code to simulate the longitudinal free water transfer during drying of oak wood. Convective longitudinal drying experiments performed on this type of wood are compared to the computational data. Results indicate that the film flow approach seems to describe the free water transport correctly in the overall non-hygroscopic domain. © 2002 Elsevier Science B.V. All rights reserved.

Keywords: Capillary porous medium; Films; Drying; Irreducible saturation; Relative permeabilities

1. Introduction

Physical phenomena involved during drying of a hygroscopic capillary porous medium have often been discussed for the last 20 years. In most of the studies, physical models used to describe moisture transfer are based on the existence of two different regions referred to as "non-hygroscopic region" and "hygroscopic region". This last region is characterized by the exclusive presence of bound water [1,2]. In the non-hygroscopic region, free liquid water occupies the major portion of the pores in the medium and is retained by capillary forces. In both regions, bound water is physically adsorbed on the walls of the solid structure by van der Waals or electrostatic forces under the form of multimolecular layers.

To estimate the titrable water content present in the medium, one usually uses the dry-based moisture content, W, defined as the mass of titrable water to the mass of dry product ratio. In addition, one also uses the water saturation, S, which locally represents the free water volume to the pore volume ratio.

During drying, free water is first eliminated thanks to the action of capillary forces until the local saturation falls to zero. At this point, no more free water locally exists but the solid structure is still saturated with bound water. The bound water content is actually to its maximum value, W_{sp},

corresponding to the saturation point of the solid matrix. Below this saturation point, bound water removal starts.

In the non-hygroscopic region, two different sub-regions are often distinguished in the literature: the "funicular" and "pendular" regions. The limit between these two regions is often called irreducible saturation point at which $S = S_{irr}$ [3–6]. In the funicular zone ($S \geq S_{irr}$) free water transfer is described by a generalized Darcy's law. In the pendular zone ($0 \leq S \leq S_{irr}$) two different approaches have been proposed in the literature to describe free water transfer: one using a saturation jump [4,7], and the other one based on a generalized Darcy's law obtained as an extension of capillary pressure and liquid relative permeability from $S = S_{irr}$ to $S = 0$ [8,9]. In our opinion, this extension of Darcy's law in the "pendular" region is physically justified for a hygroscopic medium since the presence of bound water insures continuity of the liquid phase through connected wetting liquid films.

Our aim in this work is to justify the use of a generalized Darcy's law for free water momentum transfer during drying of a capillary porous medium in the overall non-hygroscopic domain. With this goal in view, and in order to learn more about the role of liquid films during drying of a hygroscopic medium, drying experiments were performed on a capillary tube of rectangular cross section. During these experiments, the displacement of a water/vapor meniscus, resulting from a controlled drying flux applied at an open end of the tube, was followed. These experiments clearly indicate the presence of wetting films connecting the meniscus to the solid walls (see Appendix A). This brings further arguments suggesting that connected liquid films are able to ensure free water flow in the non-hygroscopic region. As a conse-

* Corresponding author. Tel.: +33-5-56-84-54-29;
fax: +33-5-56-84-54-01.
E-mail address: goyeneche@lept-ensam.u-bordeaux.fr (M. Goyeneche).
[1] Tel.: +33-5-56-84-63-64; fax: +33-5-56-84-66-45.

Nomenclature

C	mass fraction of the vapor in the gas phase
C_p	constant pressure heat capacity (J/kg K)
D	diffusivity (m^2/s)
e	film thickness (m)
F_m	mass flux (kg/m^2 s)
$\boldsymbol{g}$	acceleration due to gravity (m/s^2)
h	intrinsic averaged enthalpy (J/kg)
H	double mean curvature of α–β interface (m^{-1})
H_m	mass transfer coefficient (m/s)
H_T	heat transfer coefficient (W/m^2 K)
$\boldsymbol{J}$	flux (kg/m^2 s or J/m^2 s)
K	intrinsic permeability (m^2)
K_κ	volumetric mass rate of evaporation (kg/m^3 s)
$K_{r\kappa}$	κ-phase relative permeability
$K_{r\kappa\xi}$	κ-phase/ξ-phase coupling relative permeability
L_0	characteristic length of a capillary tube (m)
$\boldsymbol{n}_{\beta\alpha}$	unit normal vector to the $A_{\alpha\beta}$ interface directed from the β-phase to the α-phase
p	pressure (kg/m s^2)
Q	total heat flux (W/m^2)
R_0	mean capillary radius (m)
S	free water saturation
S_{irr}	irreducible saturation
T	temperature (K)
u_κ	κ-phase axial velocity in the capillary tube (m/s)
$\boldsymbol{V}_\kappa$	κ-phase local velocity in the capillary tube (m/s)
$\bar{\boldsymbol{V}}_\kappa$	κ-phase filtration velocity for a hygroscopic capillary porous medium (m/s)
W	dry-based moisture content
W_{sp}	dry-based bound water content at the saturation point

Greek symbols

α	gas phase
β	liquid phase
ϕ	porosity measured on a dry sample
γ	water superficial tension (N/m)
λ	effective thermal conductivity (W/m K)
μ_κ	dynamic viscosity (kg/m s)
ρ	apparent density (kg/m^3)
σ	solid phase
Σ	stress tensor

Subscripts

a	dry air
b	bound water
c	capillary
inf	drying air environment
m	macroscopic mean value
v	vapor
α	gas (humid air)
β	liquid (free water)
σ	solid

Superscript

g	gas

Mathematical operators

tilde ($\tilde{}$)	dimensionless variable
bar ($\bar{}$)	average value of a quantity ψ

quence, a film flow model is first developed on a cylindrical capillary tube. By putting forth some assumptions related to the geometry of the porous medium and the distribution of free water in the liquid films, this film flow model allows to predict the relative permeability–saturation relationships without any other adjustable parameter. This result is then inserted in a numerical drying model. Numerical results are finally compared with those obtained from convective drying experiments performed on oak wood in the longitudinal direction. This comparison confirms the film flow mechanism as a physically relevant one and justifies the use of a generalized Darcy's law in the overall non-hygroscopic domain.

2. Film flow model

In this section, a film flow model is proposed in order to describe free water transfer in a hygroscopic porous medium. First, the two-phase Stokes problem is solved in a single capillary tube. The film flow model is then extended to the case of a bundle of capillary tubes. To do so, free water is assumed to be distributed under the form of wetting films, and gas phase is assumed to occupy the center of the pores, allowing the estimation of relative permeability–saturation relationships that are further used for numerical simulations.

2.1. A film flow model in a cylindrical capillary tube

The configuration under concern is depicted in Fig. 1 where we have represented a cylindrical capillary tube (σ-phase) of length L_0 having a circular cross section of inner radius R_0.
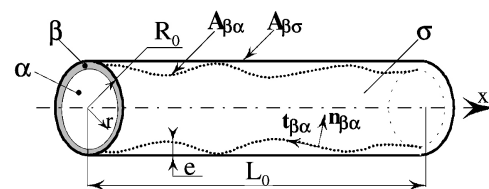

Fig. 1. Cylindrical capillary tube.

The inner wall is supposed to be covered by a wetting film (β-phase) of local thickness e, while the non-wetting fluid (α-phase) flows in the center of the tube. The length, L_0, is supposed to be infinitely large compared to R_0, and we assume that the problem is axisymmetric, stationary and that both phases are Newtonian and incompressible. Flow is supposed to occur at a sufficiently low Reynolds number for the Stokes approximation to remain valid.

In the following, we neglect van der Waals and electrostatic forces and we further and assume that no shear and phase-change occur on the α–β interface. Surface elasticity, surface viscosity, and convective momentum transport are supposed to be negligible on this surface. The set of equations for the two-phase flow is hence given as follows:

- α- and β-phases:

$$\nabla \cdot \boldsymbol{V}_\kappa = 0 \tag{1}$$

$$\nabla p_\kappa = \mu_\kappa \nabla^2 \boldsymbol{V}_\kappa \tag{2}$$

- α–β interface ($r = R_0 - e(x)$):

$$\boldsymbol{V}_\alpha = \boldsymbol{V}_\beta \tag{3}$$

$$[\boldsymbol{n}_{\beta\alpha} \cdot \Sigma] = \boldsymbol{n}_{\beta\alpha} \cdot (\Sigma_\beta - \Sigma_\alpha) = \gamma H \boldsymbol{n}_{\beta\alpha} \tag{4}$$

- β–σ interface ($r = R_0$):

$$\boldsymbol{V}_\beta = 0 \tag{5}$$

In order to solve this set of equations, two different approaches are used. A 1D solution is first obtained by making use of a classical lubrication approximation. This solution is then compared with the 2D solution obtained from an asymptotic development. Up to the first order in terms of the small parameter $\varepsilon = R_0/L_0$, 1D and 2D solutions are exactly identical [10] and the local gas and liquid longitudinal velocities are, respectively,

- for $0 \leq r \leq R_0(1 - \tilde{e})$:

$$
\begin{aligned}
u_\alpha(r) = {} & \frac{1}{4\mu_\alpha}\left(\frac{\mathrm{d}p_\alpha}{\mathrm{d}x}\right)\left[r^2 + 2R_0^2(1 - \tilde{e})^2\right. \\
& \times \left.\left\{\frac{\mu_\alpha}{\mu_\beta}\ln(1 - \tilde{e}) - \frac{1}{2}\right\}\right] + \frac{1}{4\mu_\beta}\left(\frac{\mathrm{d}p_\beta}{\mathrm{d}x}\right) \\
& \times \left[R_0^2(1 - \tilde{e})^2 - R_0^2 - 2R_0^2(1 - \tilde{e})^2 \ln(1 - \tilde{e})\right]
\end{aligned}
\tag{6}
$$

- for $R_0(1 - \tilde{e}) \leq r \leq R_0$:

$$
\begin{aligned}
u_\beta(r) = {} & \frac{1}{4\mu_\beta}\left(\frac{\mathrm{d}p_\beta}{\mathrm{d}x}\right)\left[r^2 - R_0^2 - 2R_0^2(1 - \tilde{e})^2 \ln\frac{r}{R_0}\right] \\
& + \frac{1}{2\mu_\beta}\left(\frac{\mathrm{d}p_\alpha}{\mathrm{d}x}\right)R_0^2(1 - \tilde{e})^2 \ln\frac{r}{R_0}
\end{aligned}
\tag{7}
$$

where $\tilde{e}$ represents the film thickness made dimensionless by R_0.

2.2. Extension of the film flow model to an ideal capillary porous medium: a network of parallel capillaries

The above results can be scaled up to an ideal capillary porous medium allowing the determination of gas and liquid filtration velocities in this type of structure. To do so, two hypotheses are further considered. The first one is a geometrical assumption and assumes that the capillary porous medium under study can be replaced by an equivalent network of parallel capillaries of circular cross section of radius R_0. With this assumption, gas and liquid filtration velocities, $\bar{V}_\alpha$ and $\bar{V}_\beta$, are obtained by spatially averaging the local velocities u_α and u_β:

$$
\begin{aligned}
\bar{V}_\alpha = {} & \frac{R_0^2\phi}{8\mu_\alpha}\left(\frac{\mathrm{d}p_\alpha}{\mathrm{d}x}\right)\left[-(1 - \tilde{e})^4 + 4\frac{\mu_\alpha}{\mu_\beta}(1 - \tilde{e})^4 \ln(1 - \tilde{e})\right] \\
& + \frac{R_0^2\phi}{4\mu_\beta}\left(\frac{\mathrm{d}p_\beta}{\mathrm{d}x}\right)\left[(1 - \tilde{e})^4 - (1 - \tilde{e})^2\right. \\
& \left. - 2(1 - \tilde{e})^4 \ln(1 - \tilde{e})\right]
\end{aligned}
\tag{8}
$$

$$
\begin{aligned}
\bar{V}_\beta = {} & \frac{R_0^2\phi}{8\mu_\beta}\left(\frac{\mathrm{d}p_\beta}{\mathrm{d}x}\right)\left[1 - (1 - \tilde{e})^4 - 2((1 - \tilde{e})^2 - 1)^2\right. \\
& \left. + 4(1 - \tilde{e})^4 \ln(1 - \tilde{e})\right] + \frac{R_0^2\phi}{4\mu_\alpha}\left(\frac{\mathrm{d}p_\alpha}{\mathrm{d}x}\right) \\
& \times \left[(1 - \tilde{e})^4 - (1 - \tilde{e})^2 - 2(1 - \tilde{e})^4 \ln(1 - \tilde{e})\right]
\end{aligned}
\tag{9}
$$

The second assumption is on the free water distribution. We suppose that all the free water is distributed under the form of liquid films covering the internal wall of the capillaries. Consequently, free water retained in pendular rings or entrapped clusters is not taken into account. By using this hypothesis, a direct relationship between free water saturation S and dimensionless film thickness, $\tilde{e}$, is obtained:

$$S(x) = \frac{\pi R_0^2 - \pi(R_0 - R_0\tilde{e}(x))^2}{\pi R_0^2} = 1 - (1 - \tilde{e}(x))^2 \tag{10}$$

2.3. Relative permeabilities in a network of parallel capillaries

Our interest is now to estimate the relative permeabilities for the two-phase flow considered in this paper. To do so, gas and liquid filtration velocities (Eqs. (8) and (9)) are compared with a generalized Darcy's law. By a direct identification procedure, we obtain the relative permeabilities in terms of free water saturation:

$$K_{r\alpha} = (1 - S)^2\left(1 - 2\frac{\mu_\alpha}{\mu_\beta}\ln(1 - S)\right) \tag{11}$$

$$K_{r\beta} = S(3S - 2) - 2(1 - S)^2 \ln(1 - S) \tag{12}$$

These expressions having the expecting asymptotic behavior in agreement with results of [11]. One can also note that the gas relative permeability depends on the viscosity ratio of

the two phases while the liquid relative permeability does not.

The main advantage of these relative permeability expressions is their predictive character with no particular adjustment in contrast with existing works where these parameters were adjusted from experimental results [11].

3. Integration of the film flow model in a drying numerical code

The aim of this section is to test the ability of our film flow model to describe the moisture transport in the non-hygroscopic region ($0 \leq S \leq 1$) during drying of a hygroscopic capillary porous medium. To do so, the relative permeabilities determined above are inserted in a complete numerical drying code. To check the physical relevance of this model, 1D convective drying experiments were performed on samples of oak wood and experimental results were compared with those obtained from the numerical simulations.

To perform our test, oak wood was chosen for two main reasons: (i) thermo-physical characteristics of the structure of this wood have been previously determined [12] and (ii) in the fiber direction, oak wood has a structure that allows a reasonable representation by a bundle of parallel capillary tubes [13].

In this work, we use a numerical code detailed elsewhere [11] in order to describe moisture transfer during drying of a hygroscopic capillary porous medium. At the pore scale, the system is composed of a solid phase (which is assumed to be rigid), bound water, a liquid phase (free water) and a gas phase containing both dry air and water vapor. Starting from a general mathematical description at the pore-scale of heat and mass transport processes, a volume averaging technique can be used to obtain a drying model at the Darcy's scale. The corresponding equations for mass and energy transfers are as follows [14]:

$$\frac{\partial U}{\partial t} + \nabla \cdot \boldsymbol{J} = q \tag{13}$$

with

for solid : $\quad U = \bar{\rho}_\sigma, \qquad \boldsymbol{J} = 0, \qquad q = 0$

for dry air : $\quad U = \bar{\rho}_a, \qquad \boldsymbol{J} = \bar{\rho}_a^\alpha \bar{V}_a, \qquad q = 0$

for vapor : $\quad U = \bar{\rho}_v, \qquad \boldsymbol{J} = \bar{\rho}_v^\alpha \bar{V}_v, \qquad q = K_\beta + K_b$

for free water : $\quad U = \bar{\rho}_\beta, \qquad \boldsymbol{J} = \bar{\rho}_\beta^\beta \bar{V}_\beta, \qquad q = -K_\beta$

for bound water : $\quad U = \bar{\rho}_b, \qquad \boldsymbol{J} = \overline{\boldsymbol{\rho}_b \boldsymbol{V}_b}, \qquad q = -K_b$

for energy : $\quad U = \bar{\rho}_\sigma h_\sigma + \bar{\rho}_a h_a + \bar{\rho}_v h_v + \bar{\rho}_\beta h_\beta + \bar{\rho}_b \bar{h}_b,$
$\boldsymbol{J} = \bar{\rho}_a^\alpha \bar{V}_a h_a + \bar{\rho}_v^\alpha \bar{V}_v h_v + \bar{\rho}_\beta^\beta \bar{V}_\beta h_\beta + \overline{\boldsymbol{\rho}_b \boldsymbol{V}_b \boldsymbol{h}_b} - \lambda \cdot \nabla \bar{T},$
$q = Q$

In the above equations, fluxes are represented as follows. For the convective gas flow, a generalized Darcy's law is used in the overall drying process:

$$\bar{V}_\alpha = -\frac{\boldsymbol{K} \cdot \boldsymbol{K}_{r\alpha}}{\mu_\alpha} \cdot (\nabla \bar{p}_\alpha^\alpha - \bar{\rho}_\alpha^\alpha \boldsymbol{g}) \tag{14}$$

while the convective liquid flow is described by a generalized Darcy's law in the overall non-hygroscopic region as follows:

$$\bar{V}_\beta = -\frac{\boldsymbol{K} \cdot \boldsymbol{K}_{r\beta}}{\mu_\beta} \cdot (\nabla \bar{p}_\alpha^\alpha - \nabla p_c - \bar{\rho}_\beta^\beta \boldsymbol{g}) \tag{15}$$

with $p_c = p_\alpha - p_\beta$.

Within the gas phase, mutual diffusion occurs between dry air and water vapor, and consequently, fluxes for these two species are, respectively, written as

$$\bar{\rho}_a^\alpha \bar{V}_a = \bar{\rho}_a^\alpha \bar{V}_\alpha + \bar{\rho}_\alpha^\alpha D_v^{\text{eff}} \nabla C \tag{16}$$

$$\bar{\rho}_v^\alpha \bar{V}_v = \bar{\rho}_v^\alpha \bar{V}_\alpha - \bar{\rho}_\alpha^\alpha D_v^{\text{eff}} \nabla C \tag{17}$$

where C is the mass fraction of vapor in the gas phase. In the hygroscopic region, bound water migration is described by a diffusion–sorption mechanism:

$$\overline{\boldsymbol{\rho}_b \boldsymbol{V}_b} = -\bar{\rho}_\sigma D_b \nabla W_b \tag{18}$$

Boundary conditions are those corresponding to convective drying and apply on gas pressure, total mass flux and total heat flux:

$$\bar{p}_\alpha^\alpha = p_{\text{inf}} \tag{19}$$

$$(\rho_\beta \bar{V}_\beta + \rho_v^\alpha V_v + \overline{\boldsymbol{\rho}_b \boldsymbol{V}_b}) \cdot \boldsymbol{n} = H_m (\bar{\rho}_v^\alpha - \rho_{v\,\text{inf}}) = F_m \tag{20}$$

$$(\bar{\rho}_a^\alpha \bar{V}_a C_{pa} \bar{T} - h_v (\rho_\beta \bar{V}_\beta + \overline{\boldsymbol{\rho}_b \boldsymbol{V}_b}) - h_b \bar{\rho}_b \bar{V}_b - \underline{\underline{\lambda}} \cdot \nabla \bar{T}) \cdot \boldsymbol{n}$$
$$= H_T (\bar{T} - T_{\text{inf}}) = Q \tag{21}$$

where H_m and H_T are the mass transfer and heat transfer coefficients, respectively.

From this set of equations, three variables can be selected to describe heat and mass transfers and in fact, gas pressure, moisture content, and temperature are usually used as unknown variables [1,6,7]. However, if average density of dry air, $\bar{\rho}_a$, and thermal mass, $\bar{H}$, are selected as unknowns instead of gas pressure and temperature, it has been shown that the resulting set of equations leads to a mathematically and physically well-posed problem [11]. With this choice, a conservative form of the problem can be derived with the advantage of an accurate agreement between continuous and discrete models and the possibility of a high performance numerical scheme.

The film flow model is introduced in the numerical model by inserting relative permeabilities (Eqs. (11) and (12)) and geometrical as well as physical characteristics of oak wood [12].
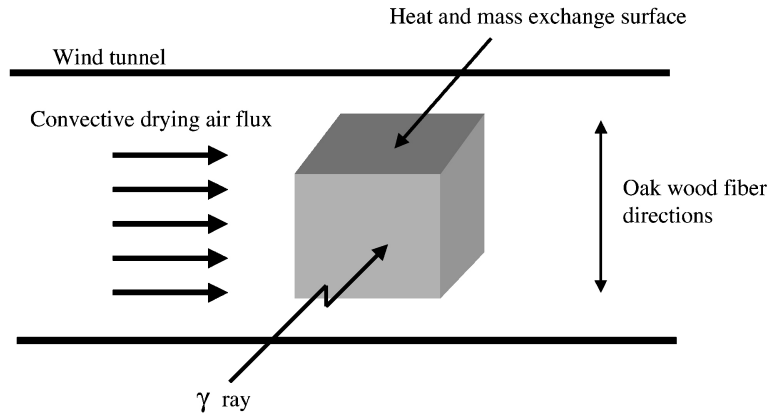
Fig. 2. A scheme of the experimental configuration.

4. Drying experiments

In order to compare numerical results, convective drying experiments were performed on oak wood. The experimental set-up is composed of a heated wind tunnel in which temperature, velocity and relative humidity of air are regulated, along with a γ-ray attenuation system mounted on a two-dimensional moving frame. Water content profiles inside the sample are obtained by measuring the attenuation of the γ-ray going through the sample and detected with a photo multiplier tube. Drying rate of the medium is obtained by weighing the sample at regular intervals of time during the experiment.

The sample is a right-angled parallelepiped. Its dimensions are 3 cm in length (longitudinal direction), 3 cm in width and 2 cm thick. Before starting the experiment, the sample is entirely saturated with water by immersion for 1 month.

In order to ensure exclusive longitudinal heat and mass transfer during drying, the upper surface of the sample only remained open; the five other surfaces (lateral and bottom surfaces) of the sample were sealed with glue (see Fig. 2). Severe drying conditions have been chosen in order to observe non-flat moisture content profiles. The sample was dried for 4 days with air at 80 °C, 15% relative humidity and 3 m/s tangential velocity over the drying surface.

5. Results and discussion

A global comparison between experimental and numerical results can be first performed in terms of drying kinetics, i.e. average moisture content versus drying time.

In Fig. 3, we have represented experimental and numerical kinetics, obtained from a spatial average of the experimental and computational time evolution of moisture content profiles, respectively. A very good agreement between the two results can be observed, except for the drying time between 1 and 8 h, for which agreement is poorer, but still fair. As a matter of fact, between 1 and 3 h of
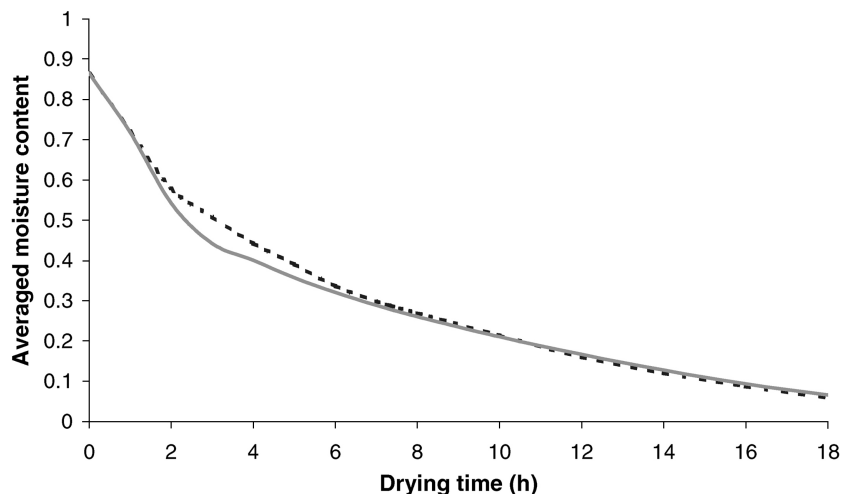

Fig. 3. Comparison of experimental (dashed line) and predicted (continuous line) moisture content vs. time.
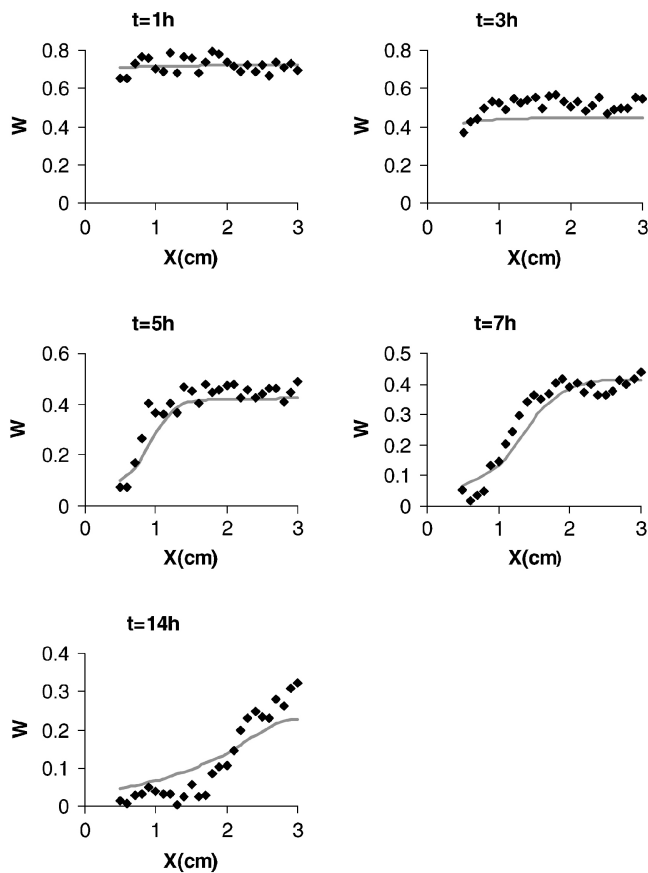
Fig. 4. Comparison of experimental (points indicated by diamonds) and predicted (continuous line) moisture content profiles during longitudinal drying of an oak wood sample.

drying, the computed drying flux is overestimated and thus, a weak discrepancy between numerical and experimental moisture content appears. Between 3 and 8 h of drying, this discrepancy becomes less significant while the computed drying flux is underestimated.

In Fig. 4, a comparison between experimental and numerical moisture content profiles is represented. Experimental moisture content profiles have been measured every 20 min in the vertical mid-section of the oak sample, each profile resulting from 26 points of γ-ray attenuation measurement. From a general point of view, experimental and numerical moisture content profiles are in good agreement.

While analyzing more precisely all the profiles during time (one profile every 20 min) a very good agreement can be observed for moisture content values greater than 0.66, which corresponds to free water saturation values greater than S_{irr}. The film flow model proposed here perfectly describes the moisture transfers in the 'funicular' zone. For moisture content values between 0.66 and 0.4, i.e. for free water saturation between S_{irr} and zero, numerical moisture contents profiles are slightly underestimated, indicating that the predicted drying rate is greater than the actual one. For these saturation values, the film flow model, as considered here, is less accurate. The assumption on free

water distribution is such that the fraction of the free water saturation retained in the pendular rings for instance is not taken into account and this may clearly explain such a discrepancy. When the entire medium is in the hygroscopic region ($W \leq W_{sp} = 0.4$), computed profiles are in good agreement with experimental ones, except at the end of the drying procedure. This final difference is however not due to the relative permeabilities since they remain constant in the hygroscopic region ($K_{r\alpha} = 0$, $K_{r\beta} = 1$). However, this last region is not studied in details here since it is beyond the scope at the present work. Nevertheless, it can be suggested that the discrepancy actually results from (i) a real difficulty to determine the effective diffusion coefficient of vapor in air as well as the effective diffusion–sorption coefficient of bound water on an experimental basis and (ii) uncertainty in the moisture content measurements with a γ-ray attenuation technique especially at low values of the water content.

6. Conclusions

A film flow model was used to describe moisture transfers in the overall non-hygroscopic region during drying of a hygroscopic capillary porous medium and, as a validation test, drying experiments were performed on oak wood.

From a general point of view, the comparison between numerical and experimental results shows a good agreement. In the non-hygroscopic region, for saturation values between $S = S_{irr}$ and $S = 0$ ($0.4 \leq W \leq 0.66$), the film flow model slightly underestimates the moisture content profiles.

In the film flow model presented in this paper, we assumed that the free water is exclusively under the form of films. This assumption seems to be correct for saturation values over S_{irr}, or in other words, provided all the free water is actually mobile. On the contrary, this hypothesis seems to be less reasonable for saturation values between $S = S_{irr}$ and $S = 0$. In this last region, a significant part of free water is trapped and should be taken into account. However, this requires further data, and, when they are available, a more detailed description based on such a film flow could be considered.

Finally, the global good performance of our predictive film flow approach leads us to suggest the two following conclusions: (i) presence of bound water in a hygroscopic medium do insure continuity of the liquid phase through connected wetting liquid films and (ii) water transfer phenomena in those films is sufficient to explain moisture transfer for small free water saturation values.

Appendix A

In order to obtain more information on the role of liquid films during drying of a hygroscopic medium, an experimental study was performed on a capillary tube partially saturated with water and subjected to a drying flux at one

Transverse section   **Longitudinal section**

Infrared radiation   Infrared radiation
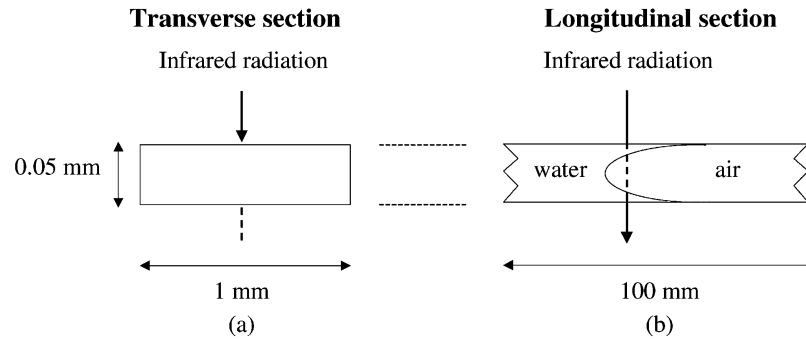

Fig. 5. Infrared radiation going through (a) an empty capillary (filled with air) and (b) a capillary with a water–air interface.
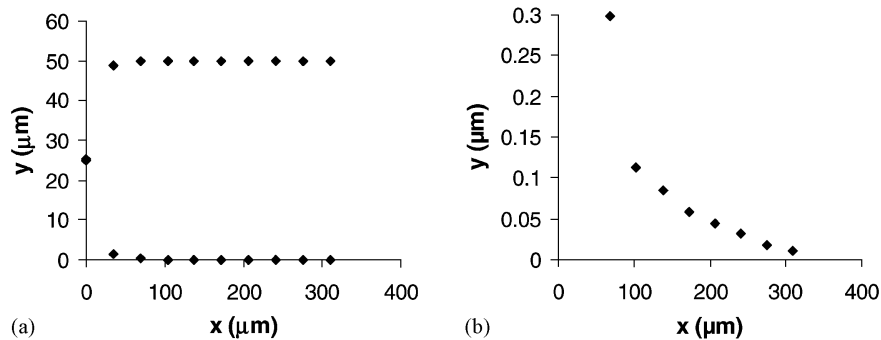

Fig. 6. (a) Form of water–air interface. (b) Zoom on the liquid film region (connection of the meniscus with the capillary walls). Temperature of drying air: 18 °C; relative humidity of drying air: 43.2%.

end. The sample, represented in Fig. 5, is a rectangular capillary tube of small dimensions (100 mm in length, 1 mm in width and 0.05 mm in thick). As a first approximation, the curvature of the meniscus in the width direction can be neglected in comparison to the curvature in the thickness direction and this is justified by the value of the aspect ratio of the tube. Moreover, in order to obtain reproducible results, ambient conditions in terms of temperature and relative humidity of the drying flux are regulated at the end of the capillary. These stationary boundary conditions are ensured by connecting this end of the capillary to a large reservoir in which the value of relative humidity is imposed by a saline solution. Experiments are performed once the system has reached equilibrium with room temperature.

The device used for the measurement is composed of an infrared spectrometer associated with an optical microscope. The measurement principle is a classical attenuation technique. First, the spectrum of the infrared radiation source transmitted through the empty and dry capillary is collected and kept as the reference spectrum. During the drying process, the water–gas interface moves in the tube and spectra of transmitted radiation through a fixed cross section of the tube are collected and stored at regular intervals of time (see Fig. 5). The ratio of these spectra with the reference spectrum provides the water thickness crossed by the infrared radiation in this section, all along the movement of the drying front (i.e. meniscus and liquid film connected to the meniscus).

The microscope has infrared and visual optics. Using the visual optics, allows one to follow the water–air interface displacement during the overall drying process providing an estimation of the velocity of the receding meniscus by a time of flight method. This interface velocity, when combined with the time evolution of the water thickness measured by using our IR attenuation system, yields the water–air interface shape. As can be seen from the result depicted in Fig. 6a, this interface is composed of two distinct regions: a 'meniscus region' and a 'film region'. A zoom of the latter represented in Fig. 6b clearly shows that the characteristic length of this film is at least two times larger than the meniscus curvature; furthermore, it clearly points out the ability of the experimental system to obtain water film thickness down to about 10 nm.

References

[1] P. Perré, A. Degiovanni, Simulations par volumes finis des transferts couplés en milieu poreux anisotropes: séchage du bois à basse et haute température, Int. J. Heat Mass Transfer 11 (33) (1990) 2463–2478.

[2] J.P. Nadeau, J.R. Puiggali, Le séchage: des processus aux procédés industriels, TEC & DOC, Lavoisier, 1995, 350 pp.

[3] G.A. Spolek, O.A. Plumb, Capillary pressure in softwoods, Wood Sci. Technol. 15 (1981) 189–199.

[4] S. Whitaker, W.T.H. Chou, Drying of granular porous media—theory and experiment, Drying Technol. 1 (1) (1983–1984) 3–33.

[5] P. Perré, C. Moyne, Processes related to drying. Part 2. Use of the same model to solve transfers both in saturated and unsaturated porous media, Drying Technol. 5 (9) (1991) 1153–1179.

[6] J.R. Puiggali, M. Quintard, Properties and simplifying assumptions for classical drying models, Adv. Drying 5 (1992) 131–147.

[7] C. Moyne, Transferts couplés chaleur-masse lors du séchage: prise en compte du mouvement de la phase gazeuse, Thesis, Nancy, France, 1987.

[8] S. Whitaker, Moisture transport mechanisms during the drying of granular porous media, in: Proceedings of the Fourth International Drying Symposium, Kyoto (Japan), July 9–12, Vol. 1, 1984, pp. 31–42.

[9] P. Perré, I.W. Turner, Transpore: a generic heat and mass transfer computational model for understanding and visualising the drying of porous media, Drying Technol. 7–8 (17) (1999) 1273–1289.

[10] M. Goyeneche, D. Lasseux, D. Bruneau, A film flow model to describe free water transport during drying of a hygroscopic capillary porous medium, Transport Por. Media, 2000, submitted for publication.

[11] F. Couture, W. Jomaa, J.R. Puiggali, Relative permeability relations: a key factor for a drying model, Transport Por. Media 23 (1996) 303–335.

[12] J.M. Hernandez, Séchage du chêne, caractérisation, procédés convectif et sous vide, Thesis, Bordeaux, France, 1991.

[13] J.F. Siau, Transport Processes in Wood, Springer Series of Wood Science, Springer, Berlin, 1984.

[14] S. Whitaker, Improved constraint for the principle of local thermal equilibrium, Ind. Eng. Chem. Res. 30 (1991) 983–997.